Group-Sparse Representation With Dictionary Learning for Medical Image Denoising and Fusion

Shutao Li*, *Member, IEEE*, Haitao Yin, and Leyuan Fang, *Student Member, IEEE*

***Abstract*—Recently, sparse representation has attracted a lot of interest in various areas. However, the standard sparse representation does not consider the intrinsic structure, i.e., the nonzero elements occur in clusters, called group sparsity. Furthermore, there is no dictionary learning method for group sparse representation considering the geometrical structure of space spanned by atoms. In this paper, we propose a novel dictionary learning method, called Dictionary Learning with Group Sparsity and Graph Regularization (DL-GSGR). First, the geometrical structure of atoms is modeled as the graph regularization. Then, combining group sparsity and graph regularization, the DL-GSGR is presented, which is solved by alternating the group sparse coding and dictionary updating. In this way, the group coherence of learned dictionary can be enforced small enough such that any signal can be group sparse coded effectively. Finally, group sparse representation with DL-GSGR is applied to 3-D medical image denoising and image fusion. Specifically, in 3-D medical image denoising, a 3-D processing mechanism (using the similarity among nearby slices) and temporal regularization (to perverse the correlations across nearby slices) are exploited. The experimental results on 3-D image denoising and image fusion demonstrate the superiority of our proposed denoising and fusion approaches.**

***Index Terms*—3-D medical image denoising, dictionary learning, graph regularization, group sparse representation, medical image fusion, temporal regularization.**

I. Introduction

MEDICAL imaging has been a useful and powerful technique for clinical investigation and disease diagnosis. However, due to the technique limitation, the quality of acquired medical images is usually unsatisfactory, which degrade the accuracy of human interpretation and further medical image analysis. Therefore, the quality of these images needs to be improved. One direct way is image denoising which receives a lot of interest. Many denoising approaches have been proposed, such as adaptive filters [1]–[3], wavelet-based methods [4]–[6], total variation-based method [7], etc. Another effective way is image fusion which can improve the quality of images by integrating the complementary information from multimodality images into a single fused image. The fused image provides accurate description of the human body and improves the diagnosis accuracy [8]. For example, magnetic resonance (MR) images can provide detailed information on soft tissue, while the dense structures like bones can be well visualized through the computed tomography (CT) technique. Fusing MR and CT images can generate the image which can describe the soft tissue and bone. The popular fusion methods are based on multiresolution analysis, such as the discrete wavelet transform [9] and stationary wavelet transform [10].

In recent years, sparse representation has emerged as a powerful tool for image denoising [11], [12], image fusion [13], [14], magnetic resonance spectroscopy [15], voxel selection [16], electroencephalogram inverse problem [17], compressive sensing [18], etc. The existing sparse representation assumes that the nonzero coefficients appear randomly. However, the sparse coefficients often exhibit intrinsic structure in form of clusters. The standard sparse representation does not consider intrinsic structure of sparse signal. Therefore, introducing the intrinsic structure into sparse representation model is a reasonable strategy to improve the performance of sparse representation [19]. In this paper, we study group sparse representation which incorporates the cluster structure into sparsity prior. It is well known that the choice of dictionary plays a crucial role in sparse representation. For the standard sparse representation, two approaches about dictionary construction are popularly used: the analytic approach (such as wavelet [20]) and the learning-based approach (such as K-SVD [21]). Currently, there are a few works focusing on dictionary learning for group sparse representation. Rosenblum *et al.* [22] proposed a dictionary learning method which is the modified version of K-SVD named as block K-SVD (BK-SVD). Different from K-SVD (rank-1 approximation), the atoms in each group are updated by the rank-k approximation in BK-SVD, where $k \geq 1$ denotes the group size. However, the BK-SVD does not consider the structure among the atoms. It is valuable to design a dictionary learning method for group sparse representation which exploits the geometrical structure among the atoms in different groups.

Recent works have shown that the graph-based method can preserve the geometrical structure effectively in manifold learning [23]. Motivated by this, utilizing the local geometrical structure of atoms and group sparsity, this paper proposes a novel dictionary learning method for group sparse representation, termed as Dictionary Learning with Group Sparsity and Graph Regularization (DL-GSGR). First, a graph is created based on group structure of the atoms in dictionary, which is described by a

Manuscript received January 9, 2012; revised April 4, 2012, July 14, 2012, and August 27, 2012; accepted August 30, 2012. Date of publication September 6, 2012; date of current version November 22, 2012. This paper was supported by the National Natural Science Foundation of China under 61172161 and the Scholarship Award for Excellent Doctoral Student granted by the Chinese Ministry of Education. *Asterisk indicates corresponding author.*

*S. Li is with the College of Electrical and Information Engineering, Hunan University, Changsha 410082, China (e-mail: shutao_li@yahoo.com.cn).

H. Yin and L. Fang are with the College of Electrical and Information Engineering, Hunan University, Changsha 410082, China (e-mail: haitao_yin@yahoo.cn; fangleyuan@gmail.com).

Color versions of one or more of the figures in this paper are available online at http://ieeexplore.ieee.org.

Digital Object Identifier 10.1109/TBME.2012.2217493

Laplacian matrix. A regularization term, called graph regularization, is presented with the Laplacian matrix. Then, combining the group sparse constraints and the graph regularization, the dictionary learning model of DL-GSGR is proposed. Finally, the proposed dictionary learning model is solved by alternating the group sparse coding and dictionary updating. Through DL-GSGR, the learned dictionary not only ensures the group sparsity, but also can preserve the local group geometrical structure of atoms. Furthermore, the group coherence of learned dictionary can be reduced through the graph regularization, which is essential for the accuracy of group sparse coding [24].

Then, the group sparse representation with DL-GSGR is applied into 3-D medical image denoising and image fusion. Generally, in 3-D medical images, the adjacent slices often exhibit the strong similarity. Using the similar slices can increase the redundancy, which is useful for noise removal. Therefore, for the task of medical image denoising, we consider the 3-D processing (several nearby slices are performed jointly) instead of 2-D processing (each slice is performed separately). To enforce the relationship among the neighboring slices, a regularization term called temporal regularization is incorporated into the 3-D denoising model. Combining the group sparsity and temporal regularization, the proposed 3-D medical image denoising method exhibits three advantages: 1) the group sparsity is more robust than standard sparsity; 2) 3-D processing utilizing the correlations among nearby slices increases the redundancy, which is a reasonable way for reducing the noise; 3) the temporal regularization can preserve the relationship among the nearby slices, namely, the continuity is kept. For medical image fusion, the group sparse coefficients of multimodality medical images with respect to the learned dictionary are used to reflect the saliency. Due to the robustness of group sparsity, the group sparse representation can provide satisfactory fused result with few artifacts.

The remainder of this paper is organized as follows. In Section II, we briefly review the group sparse representation. The proposed dictionary learning algorithm is described in Section III. Applications of group sparse representation with the proposed dictionary learning method in 3-D medical image denoising, image fusion are presented in Sections IV and V, respectively. In Section VI, we draw the conclusions and discuss some future works.

II. Group Sparse Representation

Group sparse representation assumes that the signals can be approximated by a union of a few subspaces. Let $\mathcal{G} = \{G_1, G_2, \ldots, G_g\}$ be a partition of index set $\{1, 2, \ldots, m\}$, where g is the number of groups. Given a dictionary $\mathbf{D} \in \mathbb{R}^{n\times m}$, $\mathbf{D}_{G_i}$ denotes the subdictionary with columns identical to $\mathbf{D}$ in group G_i, and the atoms in each subdictionary $\mathbf{D}_{G_i}$ span a subspace. Then, any signal $\boldsymbol{x} \in \mathbb{R}^n$ can be represented as

$$\boldsymbol{x} = \mathbf{D}\boldsymbol{\alpha} = \underbrace{\left(\mathbf{D}_{G_1}\mathbf{D}_{G_2}\ldots\mathbf{D}_{G_g}\right)}_{\mathbf{D}}\underbrace{\left(\alpha_{G_1}^T\ \alpha_{G_2}^T\ldots\alpha_{G_g}^T\right)^T}_{\boldsymbol{\alpha}} \quad (1)$$

where $\boldsymbol{\alpha} \in \mathbb{R}^m$ is group sparse vector, and T denotes the transpose of vector or matrix. With group sparsity constraint, $\boldsymbol{\alpha}$ can be sought by following optimization problem

$$\min_{\boldsymbol{\alpha}} \|\boldsymbol{\alpha}\|_{2,0} \ \text{ subject to } \boldsymbol{x} = \mathbf{D}\boldsymbol{\alpha} \quad (2)$$

where $\|\boldsymbol{\alpha}\|_{2,0} = \sum_{i=1}^{g} \mathcal{I}\left(\|\boldsymbol{\alpha}_{G_i}\|_2\right)$, and $\mathcal{I}(\cdot)$ is an indicator function defined as

$$\mathcal{I}\left(\|\boldsymbol{\alpha}_{G_i}\|_2\right) = \begin{cases} 1, & \text{if } \|\boldsymbol{\alpha}_{G_i}\|_2 > 0 \\ 0, & \text{otherwise.} \end{cases} \quad (3)$$

If the signal $\boldsymbol{x}$ is corrupted by noise, i.e., $\boldsymbol{x} = \mathbf{D}\boldsymbol{\alpha} + \boldsymbol{v}$, where $\boldsymbol{v}$ is assumed as the Gaussian noise. Then, the group sparse coefficients $\boldsymbol{\alpha}$ can be solved by the following problem:

$$\min_{\boldsymbol{\alpha}} \|\boldsymbol{\alpha}\|_{2,0} \ \text{ subject to } \ \|\boldsymbol{x} - \mathbf{D}\boldsymbol{\alpha}\|_2^2 \le \varepsilon \quad (4)$$

where $\varepsilon \ge 0$ is error tolerance.

Unfortunately, the problem (4) is a combinatorial problem. This computational intractability inspires the researchers to develop suboptimal strategies, including convex relaxation and greedy algorithm. In convex approach, the $\ell_{2,0}$ norm is replaced by the $\ell_{2,1}$ norm, leading to

$$\min_{\boldsymbol{\alpha}} \|\boldsymbol{\alpha}\|_{2,1} \ \text{ subject to } \ \|\boldsymbol{x} - \mathbf{D}\boldsymbol{\alpha}\|_2^2 \le \varepsilon \quad (5)$$

where the $\ell_{2,1}$ norm is defined as $\|\boldsymbol{\alpha}\|_{2,1} = \sum_{i=1}^{g} \|\boldsymbol{\alpha}_{G_i}\|_2$. The problem (5) can be transformed as an unconstrained version referred to group Lasso [25]

$$\min_{\boldsymbol{\alpha}} \frac{1}{2}\|\boldsymbol{x} - \mathbf{D}\boldsymbol{\alpha}\|_2^2 + \mu\|\boldsymbol{\alpha}\|_{2,1}. \quad (6)$$

Group Orthogonal Matching Pursuit (GOMP) [26] is a popular greedy algorithm for group sparse representation, which derives from OMP. Different from the OMP (selecting one atom each time), the GOMP seeks the group sparse coefficients by searching the most correlative group each time.

III. Proposed Dictionary Learning Method

Motivated by dictionary learning for the standard sparse representation and recent graph-based methods, we propose a novel dictionary learning method based on group sparsity prior and local geometrical restriction.

A. Scheme of DL-GSGR

Let $\mathbf{Z} = [z_1, z_2, \ldots, z_N] \in \mathbb{R}^{n\times N}$ be a training data matrix, where $z_i \in \mathbb{R}^n$ is the ith sampled data. Our goal is to learn a dictionary $\mathbf{D} = [d_1, d_2, \ldots, d_m] \in \mathbb{R}^{n\times m}$ and sparse coefficient matrix $\boldsymbol{\Lambda} \in \mathbb{R}^{m\times N}$, such that the product of $\mathbf{D}$ and $\boldsymbol{\Lambda}$ can approximate the original data matrix $\mathbf{Z}$ efficiently. In addition, each column $\boldsymbol{\alpha}_i$ $(i = 1, 2, \ldots, N)$ of $\boldsymbol{\Lambda}$ is restricted to group sparsity. Let $\mathcal{M} = \{\mathbf{D}, \mathbf{W}\}$ be a constructed weighted graph. The vertices of graph $\mathcal{M}$ correspond to the atoms $\{d_1, d_2, \ldots, d_m\}$, and the weight matrix $\mathbf{W}$ is used to restrict the similarity between two atoms. The weight between the ith vertex d_i and jth vertex d_j are denoted as w_{ij}. With the group sparsity assumption, any signal can be approximated by a union of some subspaces expanded by atoms in each group $(\mathbf{D}_{G_i}\ (i \in \{1, 2, \ldots, g\}))$. Therefore, when the atoms d_i and d_j are in the same subspace, i.e., the same group, the weight w_{ij} should be large.

Otherwise, w_{ij} is decreased. For simplicity, the weight matrix $\mathbf{W} = (w_{ij})_{i,j=1}^{m} \in \mathbb{R}^{m\times m}$ is defined as follows

$$w_{ij} = \begin{cases} 1, & \text{if } d_i \text{ and } d_j \text{ in the same group} \\ 0, & \text{otherwise.} \end{cases} \tag{7}$$

Furthermore, the Euclidean distance $\|d_i - d_j\|_2^2$ is applied to measure the similarity of two vertices. Thus, with the weight matrix $\mathbf{W}$, the graph regularization is formulated as

$$\frac{1}{2}\sum_{i,j=1}^{m} w_{ij}\,\|\boldsymbol{d}_i - \boldsymbol{d}_j\|_2^2 = \sum_{i=1}^{m} \boldsymbol{d}_i^T w_{ii}\boldsymbol{d}_i - \sum_{i,j=1}^{m} \boldsymbol{d}_i^T w_{ij}\boldsymbol{d}_j$$
$$= \mathrm{Tr}\left(\mathbf{DCD}^T\right) - \mathrm{Tr}\left(\mathbf{DWD}^T\right) = \mathrm{Tr}\left(\mathbf{DLD}^T\right) \tag{8}$$

where $\mathbf{C}$ is the diagonal matrix, $\mathbf{C}_{ii} = \sum_{j=1}^{m} w_{ij}$, $\mathbf{L}$ is the Laplacian matrix computed as $\mathbf{L} = \mathbf{C} - \mathbf{W}$, and Tr is the trace of a matrix. It can be seen that (8) is the sum of difference between two atoms (d_i and d_j) in the same group. Hence, minimizing (8) can reduce the difference between d_i and d_j in the same group, i.e., the similarity in same group is restrained. Conversely, the dissimilarity in different groups can be enforced. Therefore, this graph regularization can ensure the group coherence of learned dictionary small enough which is essential for group sparse coding [24]. Combining the group sparsity assumption and graph regularization, we propose a novel dictionary learning model

$$\min_{\mathbf{D},\mathbf{\Lambda}} \mu\sum_{i=1}^{N} \|\boldsymbol{\alpha}_i\|_{2,0} + \sum_{i=1}^{N} \|z_i - \mathbf{D}\boldsymbol{\alpha}_i\|_2^2 + \lambda\mathrm{Tr}\left(\mathbf{DLD}^T\right) \tag{9}$$

where $\mathbf{\Lambda} = (\boldsymbol{\alpha}_1, \boldsymbol{\alpha}_2, \ldots, \boldsymbol{\alpha}_N)$, μ and λ are regularization parameters. In model (9), the first term measures the group sparsity level, the second term controls the approximation error, and the last term is the graph regularization. The model (9) can be alternated as

$$\min_{\mathbf{D},\mathbf{\Lambda}} \|\mathbf{Z} - \mathbf{D\Lambda}\|_F^2 + \lambda\mathrm{Tr}\left(\mathbf{DLD}^T\right)$$
$$\text{subject to } \forall i \ \ \|\boldsymbol{\alpha}_i\|_{2,0} \le \tau \tag{10}$$

where τ is a natural number controlling the group sparsity level. The model (10) is equivalent to model (9) with appropriate τ.

We use an alternating strategy to solve (10) with two stages: group sparse coding and dictionary updating. In group sparse coding stage, keeping the dictionary $\mathbf{D}$ fixed, the group-sparse coefficient matrix $\mathbf{\Lambda}$ can be found by

$$\min_{\mathbf{\Lambda}} \|\mathbf{Z} - \mathbf{D\Lambda}\|_F^2 \ \text{ subject to } \forall i \ \ \|\boldsymbol{\alpha}_i\|_{2,0} \le \tau. \tag{11}$$

Due to the low complexity, we use the GOMP to solve (11) in this paper.

In dictionary updating stage, the group-sparse coefficients matrix $\mathbf{\Lambda}$ is fixed, and the dictionary $\mathbf{D}$ is updated by the following problem

$$\min_{\mathbf{D},\mathbf{\Lambda}} \|\mathbf{Z} - \mathbf{D\Lambda}\|_F^2 + \lambda\mathrm{Tr}\left(\mathbf{DLD}^T\right). \tag{12}$$

Obviously, the cost function of problem (12) is strictly convex. Therefore, taking the derivative of cost function with respect to $\mathbf{D}$ and then setting the derivation as zero yield the solution of problem (12)

$$\mathbf{D}^* = \mathbf{Z\Lambda}^T\left(\mathbf{\Lambda\Lambda}^T + \lambda\mathbf{L}\right)^{-1}. \tag{13}$$

Eventually, the whole procedures of dictionary learning method are described in Algorithm 1, termed as DL-GSGR. The applications of DL-GSGR will be stated in Section IV (3-D medical image denoising) and Section V (image fusion).

Algorithm 1: DL-GSGR

Input: Training set $\mathbf{Z}$, initial dictionary $\mathbf{D}^{(0)}$, group sparsity level τ, iterative number *Iter*, parameter λ, group partition $\mathcal{G} = \{G_1, G_2, \cdots, G_g\}$, $t = 1$, and weight matrix $\mathbf{W}$.

1. Calculate the Laplacian matrix $\mathbf{L}$

$\mathbf{L} = \mathbf{C} - \mathbf{W}$, where $\mathbf{C}_{ii} = \sum_{j=1}^{m} w_{ij}$.

2. Repeat the following steps until $t > Iter$

Group sparse coding stage:

$$\mathbf{\Lambda}^{(t)} = \arg\min_{\mathbf{\Lambda}} \left\|\mathbf{Z} - \mathbf{D}^{(t-1)}\mathbf{\Lambda}\right\|_F^2 \ \text{ subject to } \ \forall i \ \ \left\|\boldsymbol{\alpha}_i\right\|_{2,0} \le \tau.$$

Dictionary updating stage:

$$\mathbf{D}^{(t)} = \mathbf{Z}\left(\mathbf{\Lambda}^{(t)}\right)^T\left(\mathbf{\Lambda}^{(t)}\left(\mathbf{\Lambda}^{(t)}\right)^T + \lambda\mathbf{L}\right)^{-1}.$$

$t = t + 1$.

Output: Dictionary $\mathbf{D}^{(Iter)}$

B. Performance Evaluation for Dictionary Learning

In this section, the performance of DL-GSGR is evaluated by following two experiments.

1) Learning dictionary from clean training set.
2) Learning dictionary from noisy training set.

Without loss of generality, we assume that each group partition has the same group size in the following experiments. Lena image is used as the test image. The task of the first experiment is to learn two dictionaries of size 64×100 and 64×200 from clean training set, which consists of 50 000 patches of size 8×8 randomly selected from clean Lena image. In addition, the K-SVD [21] is implemented for comparison. The initial dictionaries for DL-GSGR and K-SVD are chosen as the overcomplete DCT. The fixed (group) sparsity level is used as the stopping criterions of DL-GSGR and K-SVD in (group) sparse coding stage. In this experiment, the fixed (group) sparsity level is set to 3. The RMSE is used as the objective function. The objective function values of the K-SVD and DL-GSGR (with different group size) are reported as a function of iteration number. Fig. 1(a) and (b) depicts the curves of functions for leaning dictionaries of size 64×100 and 64×200, respectively. It can see that the objective function of DL-GSGR decreases more rapidly than K-SVD.

In the second experiment, we aim to learn two dictionaries of size 64×100 and 64×200 from noisy training set, which consists of 50 000 patches of size 8×8 randomly selected from the noisy Lena image ($\sigma = 50$). The approximation error is chosen as the stopping criterions of DL-GSGR and K-SVD in (group)

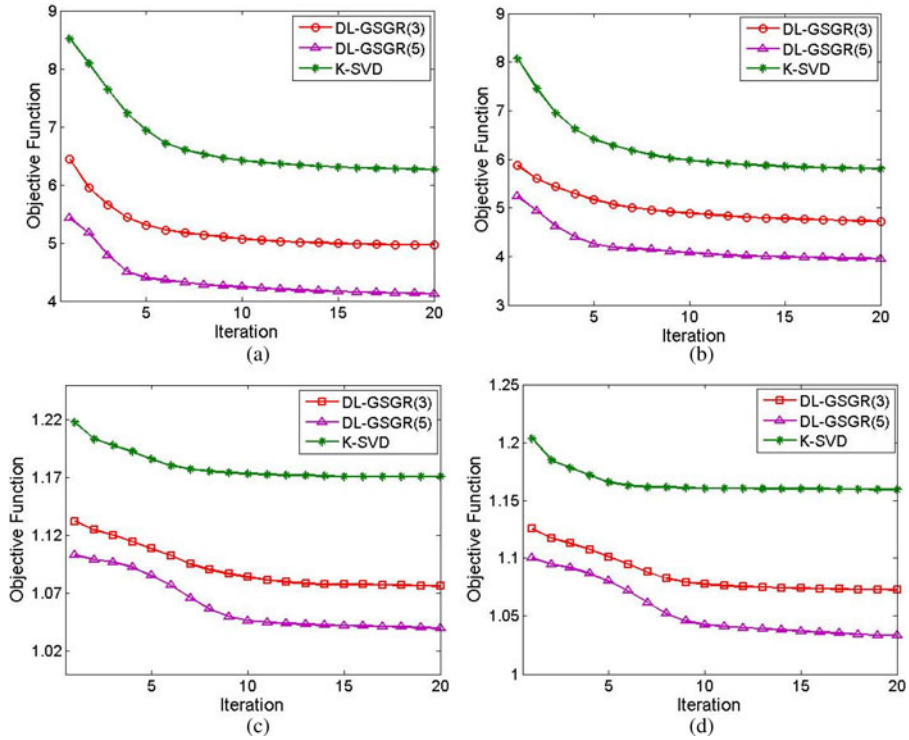

Fig. 1. Objective functions of the K-SVD and DL-GSGR (with different group size) are reported as a function of iteration number. (a) Learning dictionary of size 64×100 from clean training set. (b) Learning dictionary of size 64×200 from clean training set. (c) Learning dictionary of size 64×100 from noisy training set ($\sigma = 50$). (d) Learning dictionary of size 64×200 from noisy training set ($\sigma = 50$). DL-GSGR (3) and DL-GSGR(5) denote the DL-GSGR with group size 3 and 5. The objective function of Fig. 1(a) and (b) is RMSE, while the average number of nonzero groups and atoms for each training signal are used as objective function for K-SVD and DL-GSGR, respectively, in Fig. 1(c) and (d).

sparse coding stage, and set as $1.15 \cdot \sqrt{64} \cdot \sigma$ [11], where σ is the standard deviation. The average number of nonzero groups and atoms for each training signal is used as objective function for K-SVD and DL-GSGR, respectively. Fig. 1(c) and (d) depicts the curves of objective function value after 20 iterations of DL-GSGR and K-SVD for leaning dictionaries of size 64×100 and 64×200, respectively. Fig. 1(c) and (d) shows that the objective function of DL-GSGR decreases more rapidly than K-SVD with the same stopping criterion. Furthermore, the evaluation measure of DL-GSGR with larger group size decreases more rapidly than smaller group size, but the number of atoms used for representing a signal may be larger due to each group having more entries. To balance the number of nonzero groups and number of nonzero entries, the group size 5 is used in the following experiments.

IV. 3-D Medical Image Denoising

A. 3-D Medical Image Denoising Model

In this section, the DL-GSGR will be applied in 3-D medical image denoising. Let $\mathbf{X} \in \mathbb{R}^{N \times M \times K}$ and $\mathbf{Y} \in \mathbb{R}^{N \times M \times K}$ be the clean and noisy 3-D medical image, respectively. Generally, the MR images are modeled as a Rician distribution [27]. Hence, the noise in MR images is called as the Rician noise which is local signal dependent. For high signal-to-noise-ratio (SNR) region, the Rician distribution can be approximated by Gaussian distribution effectively. The CT images are corrupted by Poisson noise easily. However, through the variance stability transform (VST), the Poisson noise can be approximated by the Gaussian noise [28]. Therefore, we assume that the noisy medical image is formulated as $\mathbf{Y} = \mathbf{X} + \mathbf{V}$, where $\mathbf{V} \in \mathbb{R}^{N \times M \times K}$ is the Gaussian noise with standard deviation σ. The task of 3-D image denoising is to reconstruct the volumetric data $\mathbf{X}$ from $\mathbf{Y}$. In the following, a new 3-D image denoising model is designed based on the group sparse representation with DL-GSGR, termed as 3-D Denoising with Group Sparsity and Temporal Regularization (3-D DGSTR).

Following the previous work [11], the local patches are considered instead of the whole image. Let $\boldsymbol{y}_i^k = \mathbf{R}_i^k \mathbf{Y}$ be the ith patch with a square area of n pixels extracted from the kth slice of noisy medical image $\mathbf{Y}$, and ordered as n-dimension column vector, where $\mathbf{R}_i^k$ is a binary matrix extracting the patch from 3-D image. Generally, the similarity among the nearby slices exists in 3-D medical image. Therefore, we exploit a 3-D processing mechanism, namely p slices are processed jointly. Let $\boldsymbol{\mathcal{Y}}_i^k = ((\boldsymbol{y}_i^k)^T, (\boldsymbol{y}_i^{k+1})^T, \ldots, (\boldsymbol{y}_i^{k+p-1})^T)^T \in \mathbb{R}^{np}$ be the ith local 3-D patch with respect to the kth slice and nearby p slices. For the 3-D patch $\boldsymbol{\mathcal{Y}}_i^k$, the model of 3-D DGSTR is

$$\min_{\boldsymbol{\alpha}} \mu \|\boldsymbol{\alpha}\|_{2,0} + \left\|\boldsymbol{\mathcal{Y}}_i^k - \mathbf{D}\boldsymbol{\alpha}\right\|_2^2 + \lambda \sum_{j=1}^{p} \sum_{l=1}^{p} \left\|\boldsymbol{x}_i^{k+j-1} - \boldsymbol{x}_i^{k+l-1}\right\|_2^2 \quad (14)$$

where $\boldsymbol{x}_i^{k+j-1}$ $(j = 1, 2, \ldots, p)$ is the denoised patch corresponding to $\boldsymbol{y}_i^{k+j-1}$. In the model (14), the first term $(\|\boldsymbol{\alpha}\|_{2,0})$ can enforce the group sparsity, the contribution of second term

($\|\boldsymbol{\mathcal{Y}}_i^k - \mathbf{D}\boldsymbol{\alpha}\|_2^2$) is to minimize the approximation error, and the last term ($\sum_{j=1}^{p}\sum_{l=1}^{p}\|\boldsymbol{x}_i^{k+j-1} - \boldsymbol{x}_i^{k+l-1}\|_2^2$) is termed as the temporal regularization to preserve the correlation of denoised 3-D patch. Actually, the denoised 3-D patch can be formulated as $\mathcal{X}_i^k = ((\boldsymbol{x}_i^k)^T, (\boldsymbol{x}_i^{k+1})^T, \ldots, (\boldsymbol{x}_i^{k+p-1})^T)^T = \mathbf{D}\boldsymbol{\alpha}$, then $\boldsymbol{x}_i^{k+j-1}$ can be calculated as $\boldsymbol{x}_i^{k+j-1} = \mathbf{S}_j\mathcal{X}_i^k = \mathbf{S}_j\mathbf{D}\boldsymbol{\alpha}$, where the matrix $\mathbf{S}_j$ is defined as

$$\mathbf{S}_j = \left(\mathbf{0}\ldots\mathbf{0}\ \underset{\substack{\uparrow\\ \text{the } j\text{th}}}{\mathbf{I}}\ \mathbf{0}\ \ldots\mathbf{0}\right) \in \mathbb{R}^{n\times np} \tag{15}$$

$\mathbf{0} \in \mathbb{R}^{n\times n}$ and $\mathbf{I} \in \mathbb{R}^{n\times n}$ are zero matrix and identity matrix, respectively. Therefore, the temporal regularization can be rewritten as

$$\sum_{j=1}^{p}\sum_{l=1}^{p}\left\|\boldsymbol{x}_i^{k+j-1} - \boldsymbol{x}_i^{k+l-1}\right\|_2^2 = \sum_{j=1}^{p}\sum_{l=1}^{p}\|(\mathbf{S}_j - \mathbf{S}_l)\,\mathbf{D}\boldsymbol{\alpha}\|_2^2$$

$$= \boldsymbol{\alpha}^T\mathbf{D}^T\left(\sum_{j=1}^{p}\sum_{l=1}^{p}\left(\mathbf{S}_j^l\right)^T\mathbf{S}_j^l\right)\mathbf{D}\boldsymbol{\alpha} = \boldsymbol{\alpha}^T\mathbf{D}^T\mathbf{S}\mathbf{D}\alpha \tag{16}$$

where $\mathbf{S}_j^l = \mathbf{S}_j - \mathbf{S}_l$ and $\mathbf{S} = \sum_{j=1}^{p}\sum_{l=1}^{p}\left(\mathbf{S}_j^l\right)^T\mathbf{S}_j^l$. Obviously, $\mathbf{S}$ is a symmetric matrix with full rank. Then, the matrix $\mathbf{S}$ can be decomposed as $\mathbf{S} = \mathbf{U}\mathbf{V}\mathbf{U}^T$ by the singular value decomposition. Let $\mathbf{G} = \sqrt{\mathbf{V}}\mathbf{U}^T$, then $\mathbf{S} = \mathbf{G}^T\mathbf{G}$, where $\sqrt{\mathbf{V}}$ is a diagonal matrix with the diagonal elements as the square root of the diagonal elements of $\mathbf{V}$. Hence, the temporal regularization can be expressed as $\boldsymbol{\alpha}^T\mathbf{D}^T\mathbf{S}\mathbf{D}\boldsymbol{\alpha} = \boldsymbol{\alpha}^T\mathbf{D}^T\mathbf{G}^T\mathbf{G}\mathbf{D}\boldsymbol{\alpha} = \|\mathbf{G}\mathbf{D}\boldsymbol{\alpha}\|_2^2$. Therefore, the proposed 3-D medical image denoising model (14) can be rewritten as

$$\min_{\boldsymbol{\alpha}}\mu\|\boldsymbol{\alpha}\|_{2,0} + \left\|\boldsymbol{\mathcal{Y}}_i^k - \mathbf{D}\boldsymbol{\alpha}\right\|_2^2 + \lambda\|\mathbf{G}\mathbf{D}\boldsymbol{\alpha}\|_2^2. \tag{17}$$

By introducing auxiliary variables

$$\tilde{\boldsymbol{\mathcal{Y}}}_i^k = \begin{pmatrix}\boldsymbol{\mathcal{Y}}_i^k\\ 0\end{pmatrix} \text{ and } \tilde{\mathbf{D}} = \begin{pmatrix}\mathbf{D}\\ \sqrt{\lambda}\mathbf{G}\mathbf{D}\end{pmatrix}$$

the model (17) is equivalently transformed as

$$\min_{\boldsymbol{\alpha}}\mu\|\boldsymbol{\alpha}\|_{2,0} + \left\|\tilde{\boldsymbol{\mathcal{Y}}}_i^k - \tilde{\mathbf{D}}\boldsymbol{\alpha}\right\|_2^2. \tag{18}$$

We apply the GOMP to seek the approximation solution of problem (18), and the solution is denoted as $\hat{\boldsymbol{\alpha}}$. The denoised 3-D patch $\mathcal{X}_i^k$ is calculated as $\mathbf{D}\hat{\boldsymbol{\alpha}}$. Then, each 3-D noisy patch extracted from $\mathbf{Y}$ is performed by the same way. At last, averaging the overlapping pixels yields the final denoised result. In (18), the dictionary $\mathbf{D}$ plays a crucial role, which affects the denoised results. We adopt the DL-GSGR to learn the dictionary $\mathbf{D}$ from the training set.

B. Experiments

In order to evaluate the performance of proposed 3-D medical image denoising method, experiments on synthetic MR images with the Gaussian noise and Rician noise are performed. Two images with 1-mm^3 voxel resolution are obtained from BrainWeb[1]: T1-MR ($181\times217\times181$) and T2-MR ($181\times217\times181$). The Gaussian noise with different noise levels according to the maximum intensity of test image is added in the ground truth images. Actually, if the intensity values of test images are normalized to [0,255], the 20% noise level denotes Gaussian noise with standard deviation $\sigma = 51$. Moreover, the Rician noise is simulated from Gaussian noise in complex domain. The real and imaginary parts of MR images are corrupted by Gaussian noise, and then, calculating the magnitude image yields the simulated MR images with Rician noise. Nevertheless, the 3-D DGSTR is developed based on Gaussian distribution assumption. Based on the current developed VST [29] for Rician distribution, the 3-D DGSTR can be applied to reduce the Rician noise. Therefore, in the following experiments, the "VST+3-D DGSTR" denotes that the proposed 3-D DGSTR is implemented for Ricain distributed noise. To improve the adaptability of dictionary $\mathbf{D}$ in 3-D DGSTR, the dictionary $\mathbf{D}$ is learned by DL-GSGR from the noisy image, namely the 3-D patches randomly sampled from the noisy image $\mathbf{Y}$ constitute the training set. In addition, the quality of results is evaluated by peak signal-to-noise-ratio (PSNR).

Before present the experimental results, the influences of parameters of 3-D DGSTR are studied, including the nearby slice number and the training number. The nearby slice number controls the number of neighbor slices processed jointly. The training number is related to the abundance of samples in training set. To evaluate the parameter influences, the 3-D DGSTR with different parameters is validated on T1-MR image with 20% Gaussian noise and 20% Rician noise respectively, as shown in Fig. 2. From Fig. 2(a), it can be seen that increasing the nearby slice number affects the denoised result slightly for Gaussian noise if the nearby slice number is greater than 5. On the other hand, for the Rician noise condition, five neighbor slices may generate the best result. The influence of training number is shown in Fig. 2(b). The curves indicate that the performance of 3-D DGSTR is improved with increasing the training number. But higher computational cost is needed.

First, the performance of 3-D DGSTR for the Gaussian noise is evaluated. In addition, the 3-D DGSTR is compared with several 2-D denoising methods (each slice is performed separately including the K-SVD[2] [11], BM3D[3] [2], and NLM[4] [30]) and 3-D Denoising methods (several slices are performed as a whole including 3-D K-SVD and VBM3D [31]). Based on Fig. 2, for a tradeoff, the parameters setting of 2-D K-SVD, 3-D K-SVD, and 3-D DGSTR are listed in Table I. The dictionaries used in 2-D K-SVD, 3-D K-SVD, and 3-D DGSTR are adaptively learned from the noisy image. The parameters of BM3D, VBM3D, and NLM are set to the optimal values referring to [2], [31] and [30], respectively.

[1]http://mouldy.bic.mni.mcgill.ca/brainweb/
[2]Download at: http://www.cs.technion.ac.il/~ronrubin/software.html
[3]Download at: http://www.cs.tut.fi/~foi/GCF-BM3D/
[4]Download at: http://personales.upv.es/jmanjon/denoising/nlm2d.htm

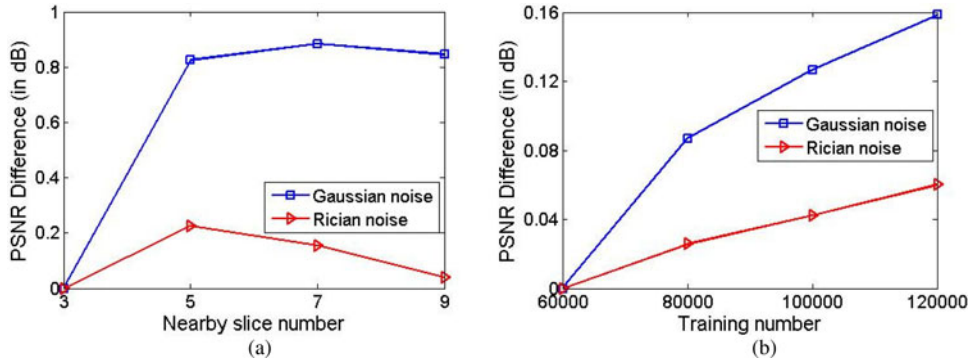

Fig. 2. Parameter influences of 3-D DGSTR for different distribution noise on the PSNR. (a) Influence of the nearby slice number. (b) Influence of the training number. The y-axis of each figure denotes the denoised results (subtract the minimum PSNR value in each type experiment).

TABLE I
PARAMETERS OF 2-D K-SVD, 3-D K-SVD, AND 3-D DGSTR

Parameters	2-D K-SVD	3-D K-SVD	3-D DGSTR
Patch size	8×8	$8\times8\times5$	$8\times8\times5$
Dictionary size	64×100	320×1000	320×1000
Initial dictionary	DCT	DCT	DCT
Training number	30000	100000	100000
Iteration	15	15	15
Group size	—	—	5

Table II presents the PSNR comparison of various methods under six different noise levels, namely 5%, 10%, 15%, 20%, 25%, and 30%. We can see that the VBM3D provides the best results in low noise level ($\sigma \leq$5% for T1-MR and $\sigma \leq$ 15% for T2-MR). However, in high noise level ($\sigma >$ 10% for T1-MR and $\sigma \geq$ 20% for T2-MR), the 3-D DGSTR matches or surpasses the VBM3D. Comparing with the 2-D denoising methods, the superiority of 3-D DGSTR is obvious. Comparing with the 3-D K-SVD, the 3-D DGSTR is superior to the 3D K-SVD in most cases. As a whole, the results of PSNR show that the proposed denoising method is effective for high noise level in two ways: 1) Comparing with 3-D K-SVD, the group sparse representation is more robust than traditional sparse representation. 2) Comparing with VBM3D, the temporal regularization can further enforce the similarity among the nearby slices. In low noise level case, the 3-D DGSTR is competitive to some popular 3-D denoising methods (3-D K-SVD, VBM3D). Figs. 3 and 4 provide a visual comparison of denoising results for T1-MR and T2-MR at 20% noise level, respectively. From the figures, it can be seen that the 3-D denoising methods generate fewer artifacts than 2-D denoising methods. Furthermore, the edge in Figs. 3(h) and 4(h) (3-D DGSTR) is sharper than Figs. 3(g) and 4(g) (3-D K-SVD), and is competitive to Figs. 3(f) and 4(f) (VBM3D).

Second, the performance of 3-D DGSTR for the Rician noise is studied. Among the methods used in the experiments of the Gaussian noise, only the NLM can be implemented with bias subtraction for Rician noise. Therefore, the "VST+3-D DGSTR" is compared with NLM for the Rician distribution data. Fig. 5 shows the 100th slice of T1 and T2-MR images, noisy images (corrupted by 20% Rician noise) and the corresponding denoised results. It can be seen that there are fewer artifacts in results by 3-D DGSTR [see Fig. 5(d) and (h)] than the results by NLM [see Fig. 5(c) and (g)]. Furthermore, the PSNR values of denoised results also demonstrate that the 3-D DGSTR is superior to the NLM.

V. MEDICAL IMAGE FUSION

A. Group Sparse Representation-Based Image Fusion

Different medical imaging devices can provide images with different body information. Medical image fusion integrates the inherent complementary information of multimodality images into one image, and thus provides a more complete and accurate description of the body. Due to the advantages of medical image fusion, it can be used for clinical diagnosis, computer-aided diagnosis, telemedicine and surgical navigation etc. Effectively and completely extracting the salient feature of multimodality images plays an important role in image fusion. The multiresolution analysis is popularly used to extract salient feature. However, each multiresolution analysis method is defined through specific mathematical model, which has its own limitation. In this paper, we propose a medical image fusion method called group sparse representation with learned dictionary-based image fusion method (GSLDF), which use the group sparse coefficients to calculate the salience level. The learned dictionary contains abundant features, such as points, lines, and corners, which can extract the salient features effectively. In GSLDF, we use the DL-GSGR to learn the dictionary. Without the loss of generality, we assume that the multimodality images are geometrically registered. If the source images are misregistered, the manual registration scheme can be used. Then, the scheme of GSLDF is summarized as follows.

1) The registered multimodality medical images $\mathbf{X}_{\boldsymbol{k}}\,(k=1,2,\ldots,K)$ are divided into overlapping patches $\left\{\boldsymbol{x}_i^k\right\}_{i=1}^{P}$ with a square area of n pixels and ordered as column vectors, where K and P are the number of images and the total patch number of each image, respectively. Each patch $\boldsymbol{x}_i^k$ minus its mean value m_i^k generates $\bar{\boldsymbol{x}}_i^k$.

TABLE II
COMPARISON OF K-SVD [11], NLM [30], BM3D [2], VBM3D [31], 3-D K-SVD, AND 3-D DGSTR FOR THE GAUSSIAN NOISE

Images	Noise Level	2-D K-SVD	NLM	BM3D	VBM3D	3-D K-SVD	3-D DGSTR
T1-MR	5%	35.24	34.75	36.09	**37.09**	36.10	36.29
	10%	31.32	30.15	32.47	**33.67**	**33.63**	**33.64**
	15%	28.86	27.62	30.24	31.61	31.57	**31.74**
	20%	27.07	25.94	28.91	29.77	30.04	**30.30**
	25%	25.72	24.71	27.77	26.76	28.85	**29.10**
	30%	24.66	23.74	26.83	25.78	27.83	**28.12**
T2-MR	5%	32.55	32.43	33.42	**34.38**	32.62	32.41
	10%	28.47	28.20	29.53	**30.82**	29.30	29.31
	15%	26.22	25.09	26.92	**28.72**	27.95	27.76
	20%	24.47	22.97	25.50	26.29	**26.51**	**26.45**
	25%	22.97	21.52	24.30	23.38	25.34	**25.41**
	30%	21.63	20.51	23.32	22.25	24.35	**24.48**

The value in bold indicates the best result in each test up to a 0.1 dB difference.

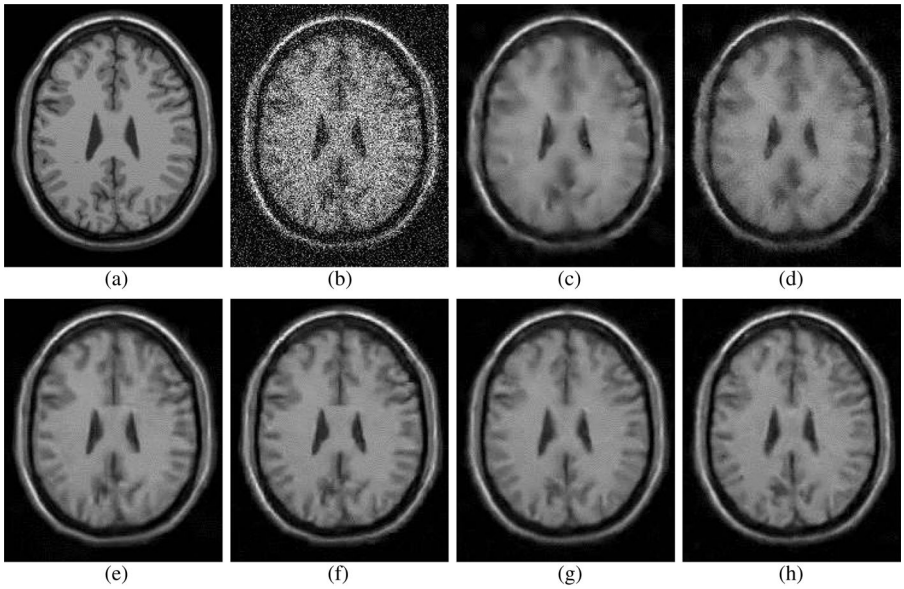

Fig. 3. Denoised results of T1-MR (slice 100) corrupted by Gaussian noise. (a) Original image. (b) Noisy image (20% noise level). (c) 2-D K-SVD. (d) NLM. (e) BM3D. (f) VBM3D. (g) 3-D K-SVD. (h) 3-D DGSTR.

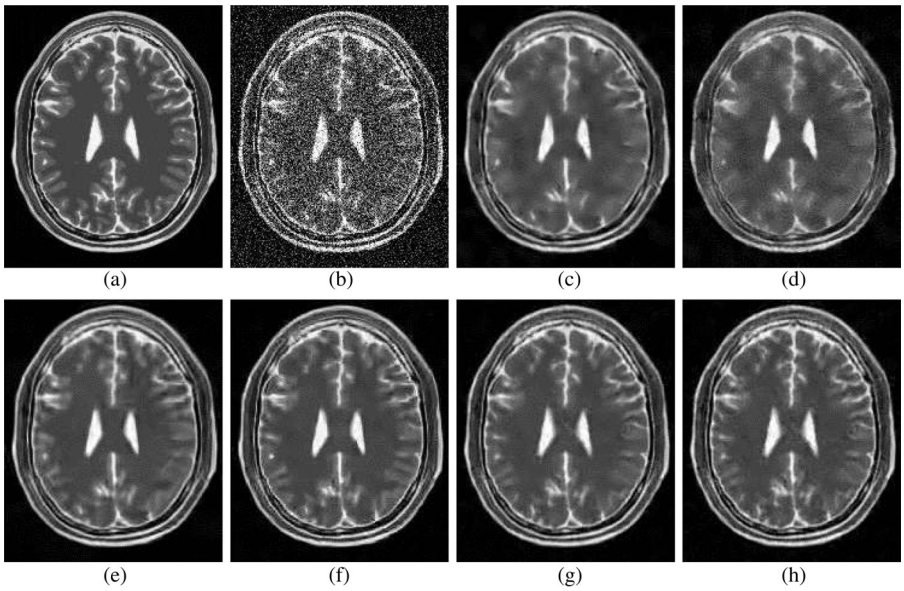

Fig. 4. Denoised results of T2-MR (slice 100) corrupted by the Gaussian noise. (a) Original image. (b) Noisy image (20% noise level). (c) 2-D K-SVD. (d) NLM. (e) BM3D. (f) VBM3D. (g) 3-D K-SVD. (h) 3-D DGSTR.

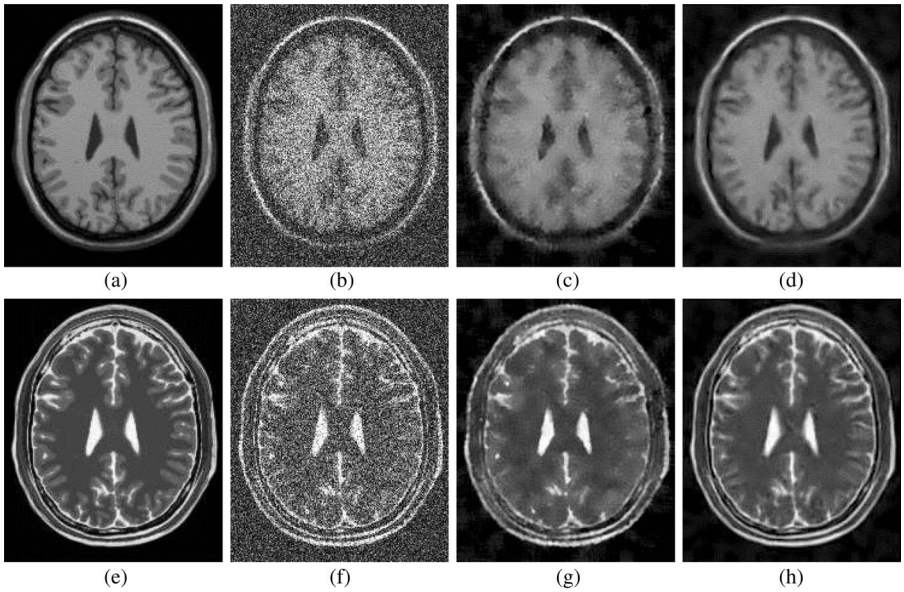

Fig. 5. Denoised results of T1/T2-MR (slice 100) corrupted by Rician noise. (a) Original T1-MR image. (b) Noisy T1-MR image (20% noise level). (c) Denoised T1-MR image by NLM (PSNR = 24.01 dB). (d) Denoised T1-MR image by 3-D DGSTR (PSNR = 24.88 dB). (e) Original T2-MR image. (f) Noisy T2-MR image (20% noise level). (g) Denoised T2-MR image by NLM (PSNR = 22.35 dB). (h) Denoised T2-MR image by 3-D DGSTR (PSNR = 24.26 dB).

2) The group sparse coefficients of each $\bar{\boldsymbol{x}}_i^k$ are sought by

$$\left(\boldsymbol{\alpha}_i^k\right)^* = \arg\min_{\boldsymbol{\alpha}_i^k} \left\|\boldsymbol{\alpha}_i^k\right\|_{2,0} \text{ subject to } \left\|\bar{\boldsymbol{x}}_i^k - \mathbf{D}\boldsymbol{\alpha}_i^k\right\|_2 \le \varepsilon,$$
$$i = 1, 2, \ldots, P; \quad k = 1, 2, \ldots, K. \tag{19}$$

The GOMP is used to solve the aforementioned optimization problem.

3) The group sparse coefficients $\left(\boldsymbol{\alpha}_i^k\right)^*$ and the mean value m_i^k $(k = 1,\ 2,\ \ldots,\ K)$ are fused by the following fusion rules

$$\boldsymbol{\alpha}_i^F = \left(\boldsymbol{\alpha}_i^{\tilde{k}}\right)^*, \quad \tilde{k} = \arg\max_{k=1,2,\ldots,K} \left\{\left\|\left(\boldsymbol{\alpha}_i^k\right)^*\right\|_2\right\} \tag{20}$$

$$m_i^F = m_i^{\hat{k}}, \quad \hat{k} = \arg\max_{k=1,2,\ldots,K} \left\{m_i^k\right\}. \tag{21}$$

4) The fused vector is computed by $\boldsymbol{x}_i^F = \mathbf{D}\boldsymbol{\alpha}_i^F + m_i^F$ $(i = 1, 2, \ldots, P)$. Then, the fused vectors are reshaped into patches with a square area of n pixels. At last, the final fused image is obtained by averaging the overlapping pixels.

B. Experimental Results

To evaluate the performance of GSLDF, the SOMP [14], SWT [10], NSCT [32], and DWT [9] based methods are performed for comparison. The patch size and dictionary size in GSLDF and SOMP based methods are set to 8×8 and 64×256. The dictionaries used in GSLDF and SOMP are learned by DL-GSGR and K-SVD offline, respectively. The training set for DL-GSGR and K-SVD is constructed by 50 000 patches randomly selected from high-quality images.[5] The decomposition level and filter for DWT and SWT are chosen as 4, and "bior 2.2," respectively. We use "pyrexc" and "dmaxflat6" as the pyramid filter and the orientation filter for NSCT, and the decomposition level is set to $\{4, 8, 8, 16\}$.

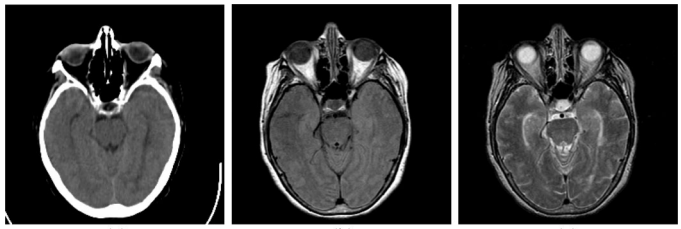

Fig. 6. Source images (slice 009). (a) CT image. (b) PD-MR image. (c) T2-MR image.

Four groups of multimodality medical images (slices 003, 006, 009, and 012) downloaded from "the whole brain"[6] are used as the source images. These images are about acute stroke of a 63 year old right-handed woman with history of hypertension and noninsulin-dependent diabetes mellitus, who complained of episodic right arm parenthesis and inability to read. Fig. 6 shows the slice 009 including CT image, PD-MR image, and T2-MR image. Obviously, the soft tissue and bone structure can be well visualized by MR (PD-MR and T2-MR) and CT images, respectively. We consider two cases: fuse CT and PD-MR images; and fuse CT and T2-MR images. To save space, Fig. 7 (fuse CT and PD-MR images) and Fig. 8 (fuse CT and

[5]Download at: http://r0k.us/graphics/kodak/

[6]Download at: http://www.med.harvard.edu/AANLIB/

Fig. 7. Results of fusing CT images and PD-MR image (slice 009). (a) DWT. (b) NSCT. (c) SOMP. (d) SWT. (e) GSLDF.

Fig. 8. Results of fusing CT images and T2-MR image (slice 009). (a) DWT. (b) NSCT. (c) SOMP. (d) SWT. (e) GSLDF.

T2-MR images) show the fused results of slice 009. The benefits of MR and CT images are merged into one image through image fusion that could provide a useful tool for surgical navigation. From Figs. 7 and 8, it can be seen that the soft tissue and bone structure (especially the pituitary, basilar artery and their surrounding structures) are preserved better with fewer artifacts by GSLDF than the compared methods. All the fused results are assessed by three clinicians who all have over five years working experience in the relevant field. They point that a clear and accurate adjacent relationship of soft tissue and bone structure is very important for intraoperative orientation. Among those fused images, they think that GSLDF provides clearer adjacent relationship and GSLDF is superior to the compared methods (the DWT-, NSCT-, SOMP-, and SWT-based methods) for surgical navigation.

For comparing objectively, five metrics including mutual information (MI) [33], universal quality index (UIQI) [34], Q_E [35], Q_W [35], and $Q^{AB/F}$ [36] are applied to assess the quality of fused results. MI computes the information transformed from the source images to the fused images. Combining loss of correlation, luminance distortion, and contrast distortion, Wang and Bovik design the UIQI. Piella and Heijmans develop the Q_E and Q_W which derive from the UIQI. Q_W gives more weight to the windows with higher saliency. Instead of original gray image considered in Q_W, Q_E evaluates the information from the original gray image and the edge image. The $Q^{AB/F}$ metric measures the edge information transferred from input images to fused image. The larger MI, Q_E, Q_W, UIQI, and $Q^{AB/F}$ values imply the better results. The chosen five fusion metrics are widely used in fusion evaluation [37], which can assess the quality of fused results reasonably in terms of information transformation, structural similarity, and feature transformation.

TABLE III
AVERAGE OBJECTIVE EVALUATION INDEXES OF DIFFERENT IMAGE FUSION METHODS

Source Images	Methods	Metrics				
		MI	Q_E	Q_W	UIQI	$Q^{AB/F}$
CT and PD-MR	DWT	2.28	0.42	0.64	0.31	0.52
	NSCT	2.33	0.46	0.67	0.34	0.60
	SOMP	2.39	0.43	0.63	0.34	**0.61**
	SWT	2.32	0.45	0.66	0.34	0.59
	GSLDF	**2.47**	**0.52**	**0.70**	**0.37**	**0.61**
CT and T2-MR	DWT	2.28	0.52	0.70	0.34	0.53
	NSCT	2.32	0.58	0.74	0.37	0.59
	SOMP	2.38	0.53	0.70	0.36	0.61
	SWT	2.31	0.57	0.74	0.36	0.59
	GSLDF	**2.45**	**0.66**	**0.80**	**0.39**	**0.62**

Table III lists the objective evaluation indexes of tested methods, which are the average values of four experiments. The values in bold indicate the best results. In the case of fusing the CT and PD-MR images, although the SOMP-based method has the same performance as our method in $Q^{AB/F}$, GSLDF generates the best results in terms of MI, Q_E, Q_W, UIQI. Furthermore, the GSLDF produces the noticeably better results in all metrics for fusing the CT and T2-MR images.

VI. CONCLUSION AND FUTURE WORKS

In this paper, we have proposed a novel dictionary learning algorithm based on group sparsity and graph regularization, namely DL-GSGR. Through DL-GSGR, the group coherence of learned dictionary can be reduced, such that any input signal can be group sparse coded effectively. Furthermore, the group sparse representation with DL-GSGR has been applied to medical image processing, including 3-D medical image denoising

and image fusion. In 3-D medical image denoising application, a 3-D processing mechanism is used to increase the redundancy, and the temporal regularization is introduced to perverse the correlations across the nearby slices. The denoising results show that our denoising method is superior to several popular 2-D denoising methods (K-SVD, NLM, and BM3D) and 3-D denoising methods (3-D K-SVD and VBM3D) in high noise level. For medical image fusion, the group sparse representation with learned dictionary (by DL-GSGR) can extract the salient feature more effectively and completely than the multiresolution analysis and the standard sparse representation. In addition, the specific defined fusion rule can preserve the complementary information effectively. The experimental results demonstrate that our fusion method surpasses the multiresolution analysis-based methods (DWT, SWT, and NSCT) and the standard sparse representation-based method (SOMP) in terms of five metrics (MI, UIQI, Q_E, Q_W, and $Q^{AB/F}$). In our future work, we will focus on the following two directions: 1) the denoising application (3-D DGSTR) to inhomogeneous noise case. 2) The fusion application (GSLDF) to simultaneous image registration and image fusion.

ACKNOWLEDGMENT

The authors would like to thank the editor and anonymous reviewers for their insightful comments and suggestions.

REFERENCES

[1] J. Oster, O. Pietquin, M. Kraemer, and J. Felblinger, "Nonlinear Bayesian filtering for denoising of electrocardiograms acquired in a magnetic resonance environment," *IEEE Trans. Biomed. Eng.*, vol. 57, no. 7, pp. 1628–1638, Jul. 2010.

[2] K. Dabov, A. Foi, V. Katkovnik, and K. Egiazarian, "Image denoising by sparse 3-D transform-domain collaborative filtering," *IEEE Trans. Image Process.*, vol. 16, no. 8, pp. 2080–2095, Aug. 2007.

[3] P. Coupé, P. Yger, S. Prima, P. Hellier, C. Kervrann, and C. Barillot, "An optimized blockwise nonlocal means denoising filter for 3-D magnetic resonance images," *IEEE Trans. Med. Imag.*, vol. 27, no. 4, pp. 425–441, Apr. 2008.

[4] H. Rabbani, R. Nezafat, and S. Gazor, "Wavelet-domain medical image denoising using bivariate Laplacian mixture model," *IEEE Trans. Biomed. Eng.*, vol. 56, no. 12, pp. 2826–2837, Dec. 2009.

[5] J. W. Lin, A. F. Laine, and S. R. Bergmann, "Improving PET-based physiological quantification through methods of wavelet denoising," *IEEE Trans. Biomed. Eng.*, vol. 48, no. 2, pp. 202–212, Feb. 2001.

[6] H. Rabbani, M. Vafadust, P. Abolmaesumi, and S. Gazor, "Speckle noise reduction of medical ultrasound images in complex wavelet domain using mixture priors," *IEEE Trans. Biomed. Eng.*, vol. 55, no. 9, pp. 2152–2160, Sep. 2008.

[7] C. S. Drapaca, "A nonlinear total variation-based denoising method with two regularization parameters," *IEEE Trans. Biomed. Eng.*, vol. 56, no. 3, pp. 582–586, Mar. 2009.

[8] B. C. Porter, D. J. Rubens, J. G. Strang, J. Smith, S. Totterman, and K. J. Parker, "Three-dimensional registration and fusion of ultrasound and MRI using major vessels as fiducial markers," *IEEE Trans. Med. Imag.*, vol. 20, no. 4, pp. 354–359, Apr. 2001.

[9] G. Pajares and J. M. de la Cruz, "A wavelet-based image fusion tutorial," *Pattern Recogn.*, vol. 37, no. 9, pp. 1855–1872, Sep. 2004.

[10] S. Li and B. Yang, "Hybrid multiresolution method for multisensor multimodal image fusion," *IEEE Sensors J.*, vol. 10, no. 9, pp. 1519–1526, Sep. 2010.

[11] M. Elad and M. Aharon, "Image denoising via sparse and redundant representations over learned dictionaries," *IEEE Trans. Image Process.*, vol. 15, no. 12, pp. 3736–3745, Dec. 2006.

[12] S. Li, L. Fang, and H. Yin, "An efficient dictionary learning algorithm and its application to 3-D medical image denoising," *IEEE Trans. Biomed. Eng.*, vol. 59, no. 2, pp. 417–427, Feb. 2012.

[13] B. Yang and S. Li, "Multifocus image fusion and restoration with sparse representation," *IEEE Trans. Instrum. Meas.*, vol. 59, no. 4, pp. 884–892, Apr. 2010.

[14] B. Yang and S. Li, "Pixel-level image fusion with simultaneous orthogonal matching pursuit," *Inf. Fusion*, vol. 13, no. 1, pp. 10–19, Jan. 2012.

[15] Y. Guo, S. Ruan, J. Landré, and J. M. Constans, "A sparse representation method for magnetic resonance spectroscopy quantification," *IEEE Trans. Biomed. Eng.*, vol. 57, no. 7, pp. 1620–1627, Jul. 2010.

[16] Y. Li, P. Namburi, Z. Yu, C. Guan, J. Feng, and Z. Gu, "Voxel selection in fMRI data analysis based on sparse representation," *IEEE Trans. Biomed. Eng.*, vol. 56, no. 10, pp. 2439–2451, Oct. 2009.

[17] P. Xu, Y. Tian, H. Chen, and D. Yao, "LP norm iterative sparse solution for EEG source localization," *IEEE Trans. Biomed. Eng.*, vol. 54, no. 3, pp. 400–409, Mar. 2007.

[18] G. Wang, Y. Bresler, and V. Ntziachristos, "Compressive sensing for biomedical imaging," *IEEE Trans. Med. Imag.*, vol. 30, no. 5, pp. 1013–1016, May 2011.

[19] J. Huang and T. Zhang, "The benefit of group sparsity," *Ann. Statist.*, vol. 38, no. 4, pp. 1978–2004, Aug. 2010.

[20] J. L. Starck, M. Elad, and D. L. Donoho, "Image decomposition via the combination of sparse representations and a variational approach," *IEEE Trans. Image Process.*, vol. 14, no. 10, pp. 1570–1582, Oct. 2005.

[21] M. Aharon, M. Elad, and A. Bruckstein, "K-SVD: An algorithm for designing overcomplete dictionaries for sparse representation," *IEEE Trans. Signal Process.*, vol. 54, no. 11, pp. 4311–4322, Nov. 2006.

[22] K. Rosenblum, L. Zelnik-Manor, and Y. C. Eldar, "Dictionary optimization for block-sparse representations," in *Proc. AAAI Fall Symp. Manifold Learning*, 2010, pp. 50–58.

[23] D. Cai, X. He, J. Han, and T. S. Huang, "Graph regularized nonnegative matrix factorization for data representation," *IEEE Trans. Pattern Anal. Mach. Intell.*, vol. 33, no. 8, pp. 1548–1560, Aug. 2011.

[24] Y. C. Eldar, P. Kuppinger, and H. Bölcskei, "Block-sparse signals: Uncertainty relations and efficient recovery," *IEEE Trans. Signal Process.*, vol. 58, no. 6, pp. 3042–3054, Jun. 2010.

[25] M. Yuan and Y. Lin, "Model selection and estimation in regression with grouped variables," *J. R. Stat. Soc. Ser. B Stat. Methodol.*, vol. 68, no. 1, pp. 49–67, Feb. 2006.

[26] A. Majumdar and R. K. Ward, "Fast group sparse classification," *Can. J. Elect. Comput. Eng.*, vol. 34, no. 4, pp. 136–144, Fall 2009.

[27] H. Gudbjartsson and S. Patz, "The Rician distribution of noisy MRI data," *Magn. Reson. Med.*, vol. 34, no. 6, pp. 910–914, Dec. 1995.

[28] F. X. Dupé, J. M. Fadili, and J. L. Starck, "A proximal iteration for deconvolving Poisson noisy images using sparse representations," *IEEE Trans. Image Process.*, vol. 18, no. 2, pp. 310–321, Feb. 2009.

[29] A. Foi, "Noise estimation and removal in MR imaging: The variance stabilization approach," in *Proc. IEEE Int. Symp. Biomed. Imag.: From Nano to Macro*, Apr. 2011, pp. 1809–1814.

[30] J. V. Manjón, J. Carbonell-Caballero, J. J. Lull, G. García-Martí, L. Martí-Bonmatí, and M. Robles, "MRI denoising using non-local means," *Med. Image Anal.*, vol. 12, no. 4, pp. 514–523, Aug. 2008.

[31] K. Dabov, A. Foi, and K. Egiazarian, "Video denoising by sparse 3D transform-domain collaborative filtering," in *Proc. European Signal Process. Conf.*, 2007, pp. 145–149.

[32] Q. Zhang and B. Guo, "Multifocus image fusion using the nonsubsampled contourlet transform," *Signal Process.*, vol. 89, no. 7, pp. 1334–1346, Jul. 2009.

[33] G. Qu, D. Zhang, and P. Yan, "Information measure for performance of image fusion," *Electron. Lett.*, vol. 38, no. 7, pp. 313–315, Mar. 2002.

[34] Z. Wang and A. C. Bovik, "A universal image quality index," *IEEE Signal Process. Lett.*, vol. 9, no. 3, pp. 81–84, Mar. 2002.

[35] G. Piella and H. Heijmans, "A new quality metric for image fusion," in *Proc. IEEE Int. Conf. Image Process.*, Sep. 2003, pp. 173–176.

[36] C. S. Xydeas and V. Petrovic, "Objective image fusion performance measure," *Electron. Lett.*, vol. 36, no. 4, pp. 308–309, Feb. 2000.

[37] Z. Liu, E. Blasch, Z. Xue, Ji. Zhao, R. Laganière, and W. Wu, "Objective assessment of multiresolution image fusion algorithms for context enhancement in night vision: A comparative study," *IEEE Trans. Pattern Anal. Mach. Intell.*, vol. 34, no. 1, pp. 94–109, Jan. 2012.

Authors' photographs and biographies not available at the time of publication.